Ninth International Conference on
THIN-WALLED STRUCTURES – ICTWS2023
Sydney, Australia, Nov 29 – Dec 1, 2023

DESIGN OPTIMISATION FOR COLD ROLLED STEEL BEAM SECTIONS WITH COMPLEX STIFFENERS CONSIDERING COLD WORKING EFFECTS

Sangar Qadir*, Van Bac Nguyen*, Iman Hajirasouliha, Martin English*****

* College of Science and Engineering, University of Derby, United Kingdom
e-mails: Sangar.Qadir@univsul.edu.iq, VB.Nguyen@derby.ac.uk

** Department of Civil and Structural Engineering, University of Sheffield, United Kingdom
e-mail: I.Hajirasouliha@sheffield.ac.uk
*** Hadley Industries plc, Downing Street, Smethwick, United Kingdom
e-mail: Martin.English@hadleygroup.com

Keywords: Cold working effect; Material testing; Cold rolled section; Complex stiffeners; Flexural strength; Finite Element modelling; Optimisation.

Abstract. *This paper presents the analysis and design optimization of the cold rolled steel sections for flexural strength considering the effect of cold working exerted on the section during the roll forming process. The sections included channel and zed shapes with complex longitudinal web and flange stiffeners. Nonlinear Finite Element (FE) modelling was developed to model the flexural strength of the channel and zed beams and validated against the four-point bending experiments for these sections. The material properties of steel at the section's flat parts, corners, and stiffener bends were obtained from tensile tests and were incorporated into the FE simulations to account for the true material properties at these regions. The section strength was then optimized using FE modelling results based on the Design of Experiments (DOE) and response surface methodology. Optimal designs for the channel and zed sections with maximum strength in distortional buckling could be obtained while changing the stiffeners' position, shape, sizes, and considering material properties at section corners and stiffener bends. It revealed that, the optimal designs provided up to 13% and 17% increase in flexural strength for the channel and zed sections, respectively; however, when the true material properties at the section corner and the stiffener's bend regions was included, the increase in flexural strength increased up to 20% and 23%, respectively.*

1 INTRODUCTION

Cold rolled beam sections, i.e., purlins in building frame systems, are usually manufactured by the cold roll forming process into conventional channel and zed profiles. These sections have a large width-to-thickness ratio, so they are prone to local or distortional buckling that govern the failure modes. A main method to improve the strength of cold rolled sections is including longitudinal stiffeners at the web and/or flange of the sections. Sections could have "standard" stiffeners such as symmetrical angle, i.e., pre-qualified profiles as defined in codes of practice [1,2] or "complex" stiffeners such as unsymmetrical angles with many curved bends or semi-circular shapes [3]. There have been extensive investigations on buckling and ultimate strengths and design of sections with web stiffeners; however, most of them are for columns under compression and there have been limited investigations on channel and zed sections with stiffeners subjected to bending [4-6]. Regarding channel and zed beams, there has been only a few studies included intermediate stiffeners in their flanges [7].

During the cold rolled forming process, significant amounts of plastic deformation are found in the regions around section corners and stiffener bends in comparison to the flat counterpart regions, hence resulting in an increase in material yield and ultimate strengths, but a decrease

in material ductility. Over the last few decades, there have been many studies conducted to quantify the cold working effect in the curved regions of metallic material and developed several models to predict the strength enhancement. The most widely used of which are for the stainless-steel sections [1-8] and the cold-formed sections [1,2,5]. Some studies have shown significant influences of cold working on load-bearing capacity of structural column members [8-11] and beam member [12].

Optimization methods including Genetic Algorithms and Particle Swarm Optimization were used together with the analytical methods available in design codes (the Effective Width Method or the Direct Strength Method) to search for optimal designs with flexural strength target [13-15]. However, this approach was rather applicable for pre-defined profiles in which the dimensions of web, flanges, lips, and stiffeners were symmetrical and, in the dimension and shape ranges required by design standards. In addition, most of previous studies on the optimization of cold rolled sections did not consider both the geometry and the cold working influences on the section strengths, resulting in not very accurate optimization results.

Only the recently published studies [16-19] utilized FE modelling and optimization techniques to determine the influences of the stiffener's geometry and cold working at the section corners and stiffener bends; the stiffener's geometry included its location, shape, and size. However, in these studies, the material properties of section corners and stiffener bends were not available from the tests. Therefore, the formulae from the North American specification [13] were used to calculate the material properties of corners and stiffener bends from those of the flat regions. While providing useful information on the effect of stiffener geometry and cold working, it did not provide accurate figures on the true material properties at section corners and stiffener bends, and subsequently, on the optimal design for flexural strength of these sections.

In this paper, the design optimization for flexural strength of cold rolled steel beam sections with intermediate stiffeners considering cold working effects at section and stiffener's corners was presented. First, four-point bending tests for channel and zed beams with complex stiffeners were conducted and material properties of at the section's flat parts, corners, and stiffener bends were obtained from tensile testing, and four-point bending tests for the same sections. Nonlinear FE models were then developed for the four-point bending tests and these models were validated against experimental test data. The verified FE models were then used for design optimization in which the Design of Experiments (DOE) and response surface techniques were used to determine the influences of geometric parameters of the section and stiffeners on the section distortional buckling and flexural strength, and a multi-objective genetic algorithm method was deployed to obtain optimal designs for flexural strength of the sections. Optimal cross-sectional shapes of the longitudinally stiffened channel and zed sections were finally selected and proposed.

2 EXPERIMENTAL TESTS

The cross sections of the test specimens are shown in Figure 1. Dimensional measurements were carried out and recorded for all test specimens prior to testing. The channel section had measured dimension as follows: a thickness of 1.23 mm, a depth of 145.04 mm, corner radius of 2.30 mm, flange's width of 63.07 mm and lip length of 16.05 mm. The zed section had measured dimension as follows: a thickness of 1.25 mm, a depth of 145.07 mm, corner radius of 2.70 mm, top flange's width of 67.00 mm and lip length of 15.02 mm, bottom flange's width of 61.03 mm and lip length of 13.89 mm.

2.1 Tensile Tests

The material properties of flat parts, corners, and stiffener bends cut from the channel and zed sections in the longitudinal direction, were obtained from tensile tests. For each type of beam section, the positions of the extracted specimens from the selected sections are shown in Figures 1(a) and 1(b). The specimen identification system begins with the specimen type (web, flange, and corner), followed by the specimen locations in the longitudinal direction for repeated tests, labelled as a, b, c. Corner specimens were taken from the section corners (web-flange junctions) at position 1; the most bent corner of the web stiffener at position 2; the second most bent corner of the web stiffener at position 3. Flat and curved steel specimens had the 'dog bone' shapes; the flat specimens had a parallel length of 75 mm and a width of 12.50 mm of the parallel length, while the curved specimens had a parallel length of 75 mm and a width ranged from 3.5 to 12.5 mm.

All tensile specimens were attached with a 50 mm gauge-length extensometer. Each specimen was instrumented with one linear 10-mm strain gauge on each side of the specimen. Due to the asymmetric shape of the curved specimens, they were tested in pairs (to avoid introducing unwanted bending moments) with a round bar with special knurled surfaces placed between the gripped ends of the specimens, as illustrated in Figure 2.

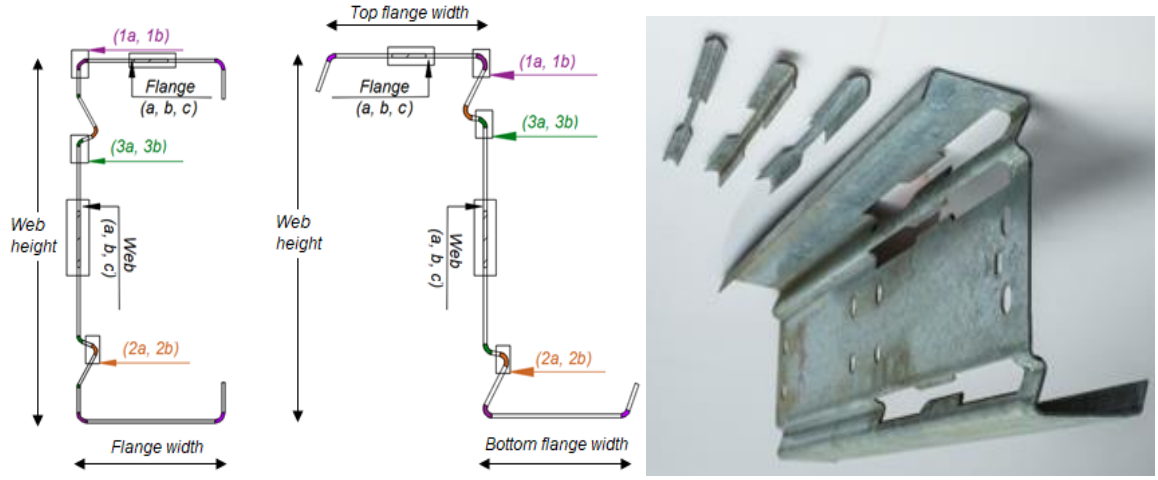

Figure 1: Locations of extracted tensile specimens (a) channel cross section, (b) zed cross section, and (c) typical curved specimens extracted from curved locations 1, 2, 3 of the zed section.

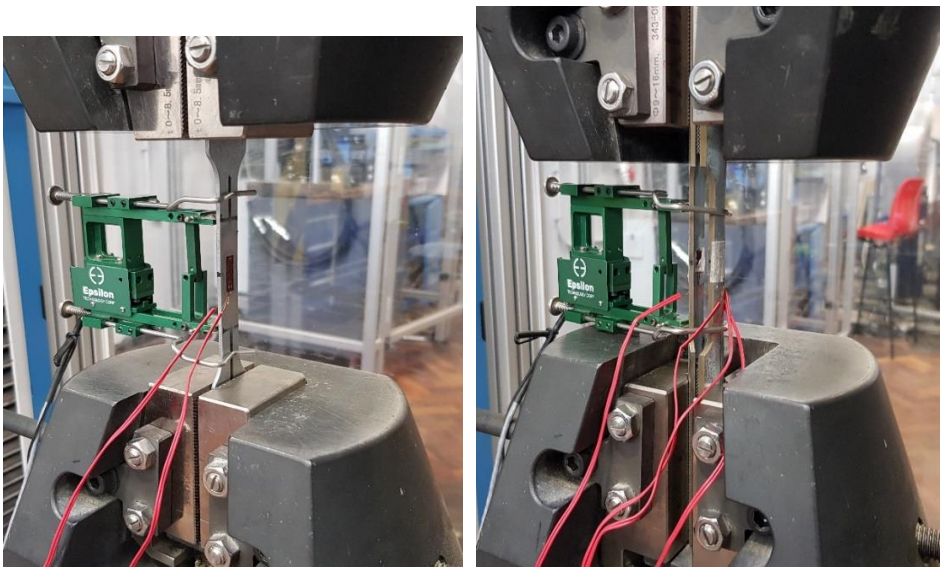

Figure 2: Typical tensile test setup (a) flat specimens and (b) curved specimens.

2.2 Bending tests

The typical test setup for the four-point bending configuration test is shown in Figure 3 (which shows the test setup of the zed sections). The beam sections were assembled in pair with lateral restraints made of 45x45 mm steel angles which were fixed by self-tapping screws to the top and bottom flanges at every distance of 500 mm, but there are no restraints on top of the sections for 1300 mm at the mid-span.

A calibrated test rig was used for the tests which consists of a 200-kN capacity hydraulic actuator. It imposed the load through a rigid I beam onto the beam specimens at two discrete locations 900 mm apart. These loads were applied through the web of the section via a bolted connection using cleats (fixed to the beam webs), which in turn contacted the load cell beams via round blocks. Round blocks were used for all supports to ensure that the reaction force/ load applied to support cleats was a point load. Electrical strain gauges were used to measure the axial strains along the web and flanges of the cross section of the beam specimens. For each section, four strain gauges were mounted on the specimen mid-span, on the perimeter outside the specimen cross section, at the web positions close to the flanges and at the centers of flanges. Displacement transducers (LVDTs) were used for determining the vertical displacements under the beams at mid-span and under the two loading points. Other LVDTs were placed at the supports to measure possible displacement in the vertical direction.

A displacement control scheme with a rate of 1 mm/min was used for all tests. The specimens were loaded to failure and the test stopped at about 70% of the ultimate load. The data associated with load, displacement and strain gauge readings were recorded by data acquisition software. To consider the variation in sample and testing conditions, two duplicated tests were carried out for each section referenced.

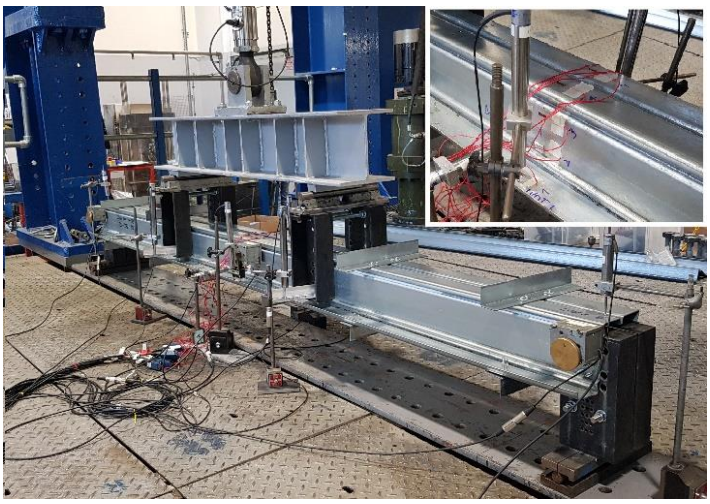

Figure 3: Four-point bending test setup, showing zed sections and strain gauge and LVDTs arrangement at mid-span of the sections (in the small box).

3 FINITE ELEMENT MODELLING AND DESIGN OPTIMIZATION

3.1 FE Modelling of the four-point bending test

FE modelling was performed using ANSYS (Version 2020R, ANSYS, Inc.) to model the four-point bending test of the channel and zed sections, as presented in Section 2. The method of developing the FE model for thin-walled sections capable of simulating the buckling and ultimate bending strength while considering the section's geometric imperfections and cold

working effects was presented in detail in Qadir et al. [19], and this method was applied to this study. The FE model setup including point load locations and boundary conditions is illustrated in Figure 4 where only half of the test system was simulated due to symmetry. The bracings were modelled using tie nodes at the symmetry plan that were rigidly connected to nodes from the top/ bottom flanges and they were constrained to prevent from movement against the transverse direction. The connections of support cleats attached to the web of the section at supports and loading points were also modelled by rigid connections between reference nodes (at center of support) and nodes at crew positions. These reference nodes were used to restrict the section ends against all the movements such as vertical, transverse and out-of-plan rotations. The reference nodes at one-third of the beams were used to apply vertical loads.

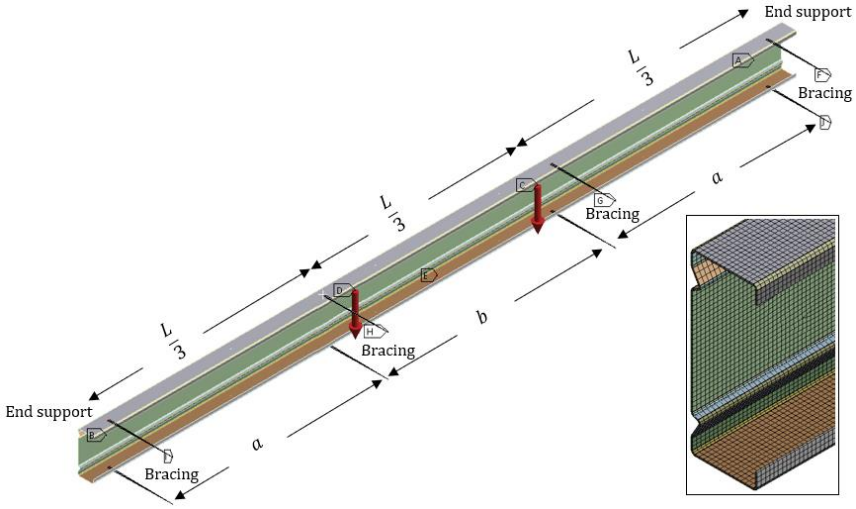

Figure 4: FE model setup which shows boundary conditions (an example of the channel section is presented) and the mesh of the section in closer view, as shown in the rectangular box.
L = 2700 mm, a = 500 mm, b = 1300 mm.

Shell elements SHELL181 which has 4-noded quadrilateral, reduced integration, were selected. The material properties for flat parts, section and stiffener's corners obtained from tensile tests (as presented in Section 2.1) were assigned in these regions of the channel and zed sections in the FE models, as shown in Figure 1. The elastic modulus E of 205,000 N/mm^2 was used. The FE modelling of the beam test included two steps. In the first step, a linear elastic buckling analysis was performed on the perfect geometry to obtain distortional buckling modes (eigenvalues). In the second step, these buckling modes were used as initial geometric imperfections for a nonlinear post-buckling analysis carried out to predict the beam behavior and ultimate load capacity. The imperfection value of 1.55t was employed for the FE analysis in this study as suggested in [17,18]. The true stress and the true strain calculated from the conventional engineering values (obtained from tensile tests), were used.

3.2 Flexural strength optimization

Figure 5 shows general dimensions for the channel and zed sections used in the optimization, which were the industrial UltraBeam^{TM2} and UltraZED^{TM2} sections, respectively (Hadley Industries plc.). The FE model validated in Section 2.2 of this paper was utilized for the optimization study. The original UltraBeam^{TM2} and UltraZED^{TM2} sections together with their bending setup were defined as "reference" sections. In the FE models of the "reference" sections, the material properties for flat parts, section and stiffener's corners were obtained from tensile tests for these sections. In the FE models of the sections used for optimization, except the section height *h* and thickness *t* were fixed, all dimensions were parameterized from P_1 to

P_{17} as shown in Figure 5. The material properties for the section corners at position 3 were used for the region of the flange stiffeners.

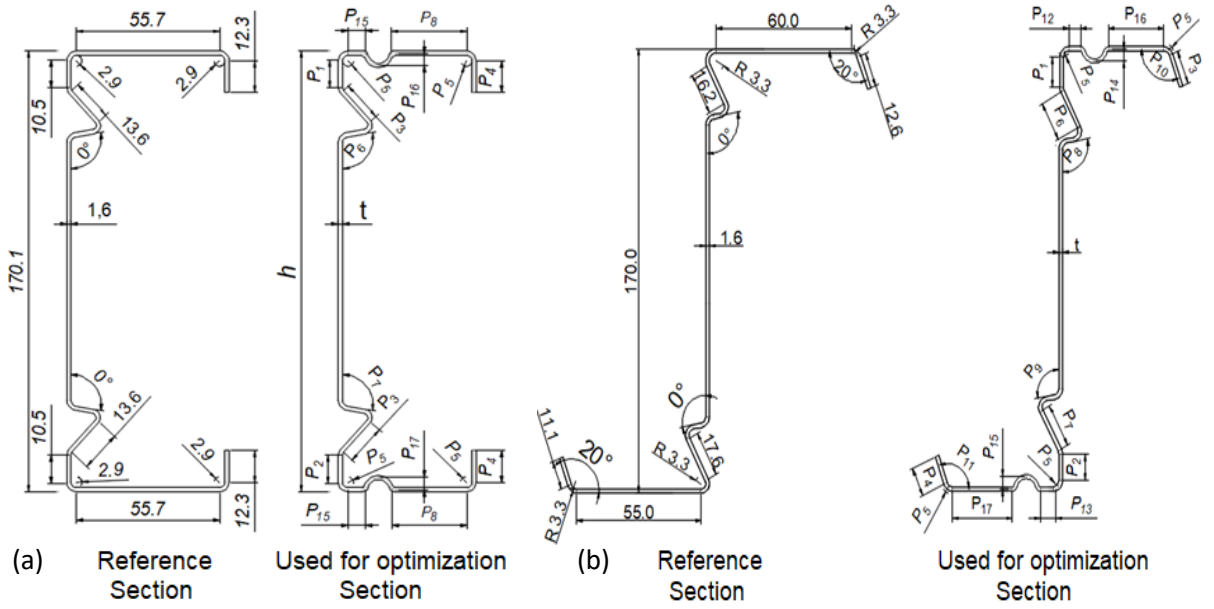

Figure 5: Dimension parameters in (mm) of "reference" sections and definition of design variables of (a) channel cross section, and (b) zed section.

The optimal cross-sectional shapes investigated in this paper, are optimized based on an optimization framework developed by the authors in the previous studies [16,19]. The proposed optimization framework takes the buckling and ultimate strength of CFS sections as objective function. A nonlinear FE model was first developed for "reference" channel and zed sections under four-point bending tests. These reference sections were then parameterized utilizing the Design of Experiment (DOE) technique in terms of geometric dimensions and material properties and the section's distortional buckling and ultimate strength were determined. In the following step, the effects of the stiffener's geometry including its location, shape, size, and material properties by the cold working at the section and stiffener's corners on section strengths were expressed through a response surface. By applying an optimization technique on these response surface data, optimal design of sections was determined based on the section's maximum ultimate strengths. For optimization target, that was "obtaining maximum strength of the section while maintaining the same weight", the total length of the cross section was kept unchanged when changing all other dimension parameters. This process resulted in generating new channel and zed shapes. Details of the method was presented in [19].

4 RESULTS AND DISCUSSION

4.1 Tensile test

Figure 6 shows the static stress-strain curves of typical flat specimens and the pair of curved specimens in Section 2.1. Stresses and strains shown in this figure are conventional engineering values. For the channel section, in comparison to the flat specimens, the yield and tensile strengths of the curved specimens were increased by 7–12% and 4–10%, respectively, and the percentage of elongation decreased by 60–70%. For the zed section, the yield and tensile strengths of the curved specimens were increased by 16–20% and 16–18%, respectively, and the percentage of elongation decreased by 43–57%. It confirmed that the cold working produced a significant increase in the yield and tensile strengths and a decrease in ductility of the section corners and stiffener's bends.

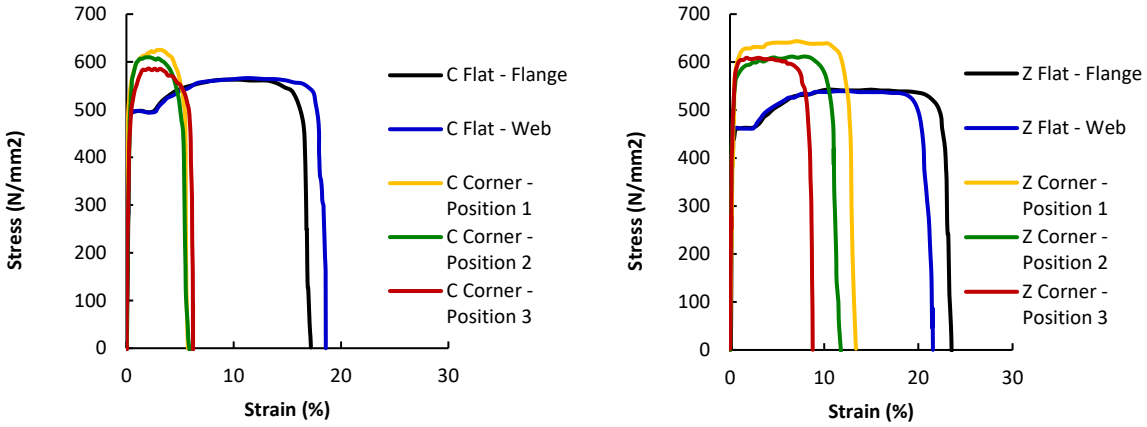

Figure 6: Engineering stress–strain relationships of flat and corner specimens for (a) channel section, and (b) zed section.

4.2 FE modelling and validation

The FE models was carried out for four-point beam bending tests conducted in Section 2.2 and the results were compared with the experimental results to validate the models. The ultimate moment capacities from experimental tests and FE models, showing the FE results were in an excellent agreement with the experimental results in terms of load-displacement curves and deformed shapes at failure, as shown in Figures 7 and 8 for channel and zed sections, respectively.

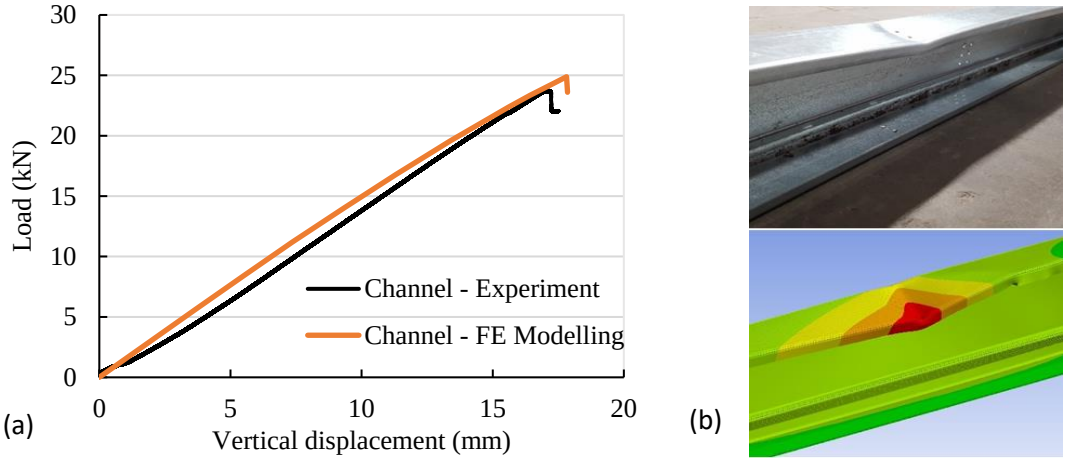

Figure 7: Experimental and FE modelling results for the channel section (a) load-displacement curves, and (b) deformed failure shapes.

4.3 Optimization for flexural strength

Table 1 summarizes the buckling and ultimate bending strengths of the cross-sectional geometries obtained from the optimization process. The resultant cross-sectional shapes and comparison between flexural strength capacity with the cold working effects and without the cold working effects of the various optimal design candidate points are also shown in Figures 9 and 10. The following observations were made from Table 1 and Figures 9 and 10:

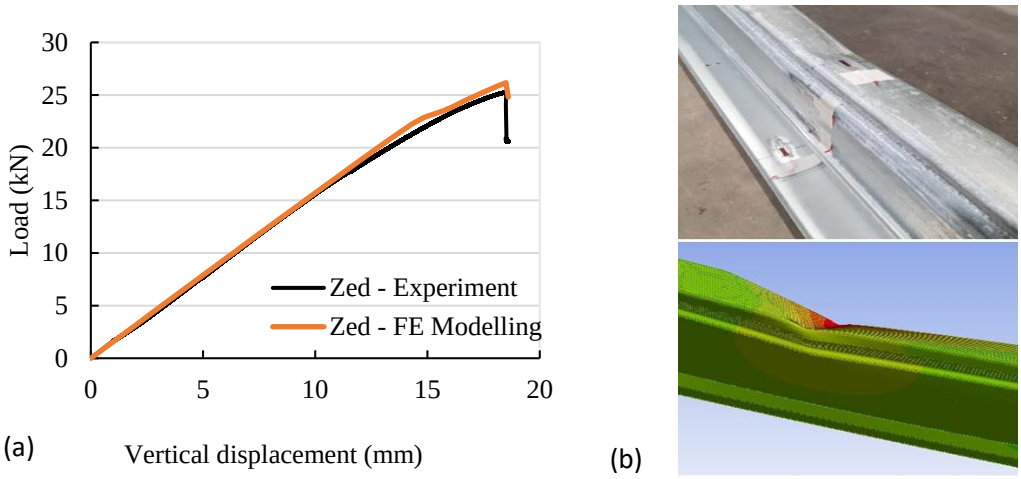

Figure 8: Experimental and FE modelling results for the zed section (a) load-displacement curves, and (b) deformed failure shapes.

Table 1: Buckling and ultimate moment capacity of standard and optimized sections. M_u, M_{uc} stands for ultimate moment capacity without and with the cold working effect, respectively.

Cross-section types	P_b (kN)	M_u (kNm)	M_{uc} (kNm)	M_{uc}/M_u	$M_{uc}/M_{uc}^{standard}$
Channel					
Standard	11.7	9.48	9.48	1.00	1.00
Reference (b)	13.4	9.48	9.63	1.02	1.02
Candidate 1	22.9	9.89	10.25	1.04	1.08
Candidate 2	23.5	9.62	9.87	1.03	1.04
Candidate 3	23.3	9.91	10.26	1.04	1.08
Reference (c)	15.3	9.67	10.26	1.07	1.08
Candidate 4	20.8	10.18	10.85	1.07	1.14
Candidate 5	23.1	10.31	10.96	1.07	1.16
Candidate 6	21.5	10.69	11.40	1.07	1.20
Zed					
Standard	9.6	9.03	9.03	1.00	1.00
Reference (b)	11.6	9.61	9.77	1.02	1.08
Candidate 1	19.7	10.38	10.55	1.02	1.17
Candidate 2	21.1	9.52	9.74	1.02	1.08
Candidate 3	20.2	10.52	11.11	1.06	1.23
Reference (c)	13.3	9.98	10.54	1.06	1.17
Candidate 4	18.8	10.38	10.91	1.05	1.21
Candidate 5	20.3	10.30	10.94	1.06	1.21
Candidate 6	19.8	10.52	11.11	1.06	1.23

• Adding two longitudinal stiffeners to the web of the sections provided significantly greater buckling strengths, by 15% and 21% for channel and zed sections, respectively, when compared to the standard sections. In terms of the ultimate moment capacities, the enhancement was noticeably improved by 2% and 8%, respectively. The cold working had noticeable effect by 2% on the reference section bending strengths.

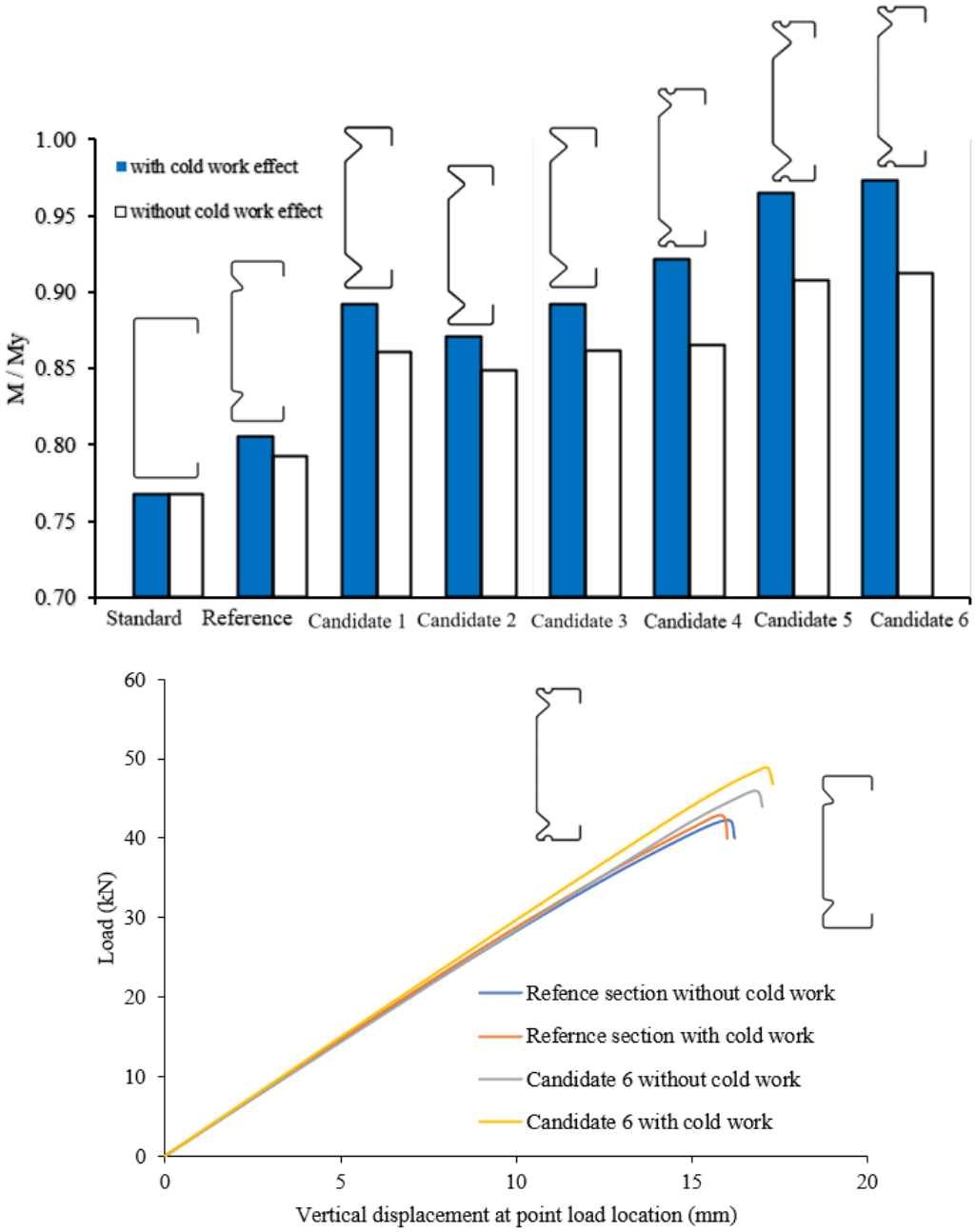

Figure 9: (a) Strength capacities with the cold working effects and without the cold working effects for channel sections, and (b) load-displacement curves for the reference section and Candidate 6.

• The optimized sections with two longitudinal web stiffeners in the web (Candidate 3) could provide with significant enhancement in the buckling of the channel sections due geometry effects which were about 100%, whereas it only considerably increased the ultimate moment capacity by 4% and extra 4% was also obtained in the ultimate moment capacity when the cold working effects were also considered. For the zed section, Candidate 3 gained significant increase in buckling strength, ultimate moment capacities considering no cold working effect, and considering cold working effect by 110%, 17% and 23%, respectively.

• The Candidate 6, the optimal solution, for both the channel and zed sections gained most increase in buckling strength, ultimate moment capacities considering no cold working effect, and considering cold working effect. They were 84%, 13% and 20% for the channel section, respectively, and 105%, 17% and 23% for the zed section, respectively.

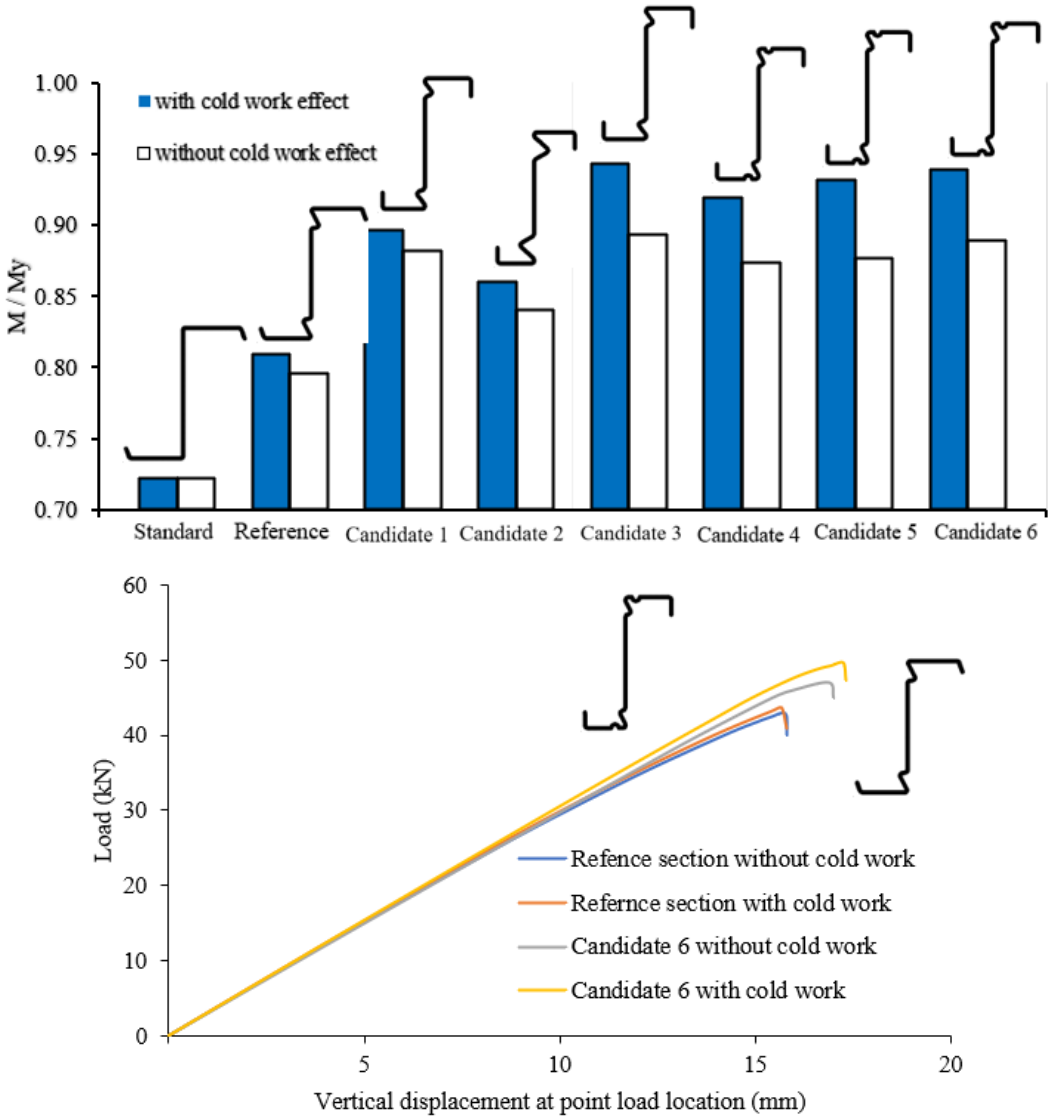

Figure 10: (a) Strength capacities with the cold working effects and without the cold working effects for zed sections, and (b) load-displacement curves for the reference section and Candidate 6.

• The optimized sections with two longitudinal web stiffeners in the web (Candidate 3) could provide with significant enhancement in the buckling of the channel sections due geometry effects which were about 100%, whereas it only considerably increased the ultimate moment capacity by 4% and extra 4% was also obtained in the ultimate moment capacity when the cold working effects were also considered. For the zed section, Candidate 3 gained significant increase in buckling strength, ultimate moment capacities considering no cold working effect, and considering cold working effect by 110%, 17% and 23%, respectively.

• The Candidate 6, the optimal solution, for both the channel and zed sections gained most increase in buckling strength, ultimate moment capacities considering no cold working effect, and considering cold working effect. They were 84%, 13% and 20% for the channel section, respectively, and 105%, 17% and 23% for the zed section, respectively.

• The Candidate 6 also exhibited a considerably increased stiffness compared to the reference sections for both the channel and zed sections, which is a direct result of the stiffeners delaying and mitigating the stiffness degradation due to buckling. It is noted that the stiffeners size was accounting for in the total developed length of the section and that, therefore, the flange width of the design candidate 6 is less than that of the reference section.

5 CONCLUSION

In this paper, the influence of cold working effects on mechanical properties and flexural strength of the cold roll formed sections were studied by experimental testing and combined Finite Element modelling and optimization. A material test program consisted of tensile tests and four-point bending tests were conducted to study the cold working effect in the section and stiffener's corners of cold roll formed sections and in the design optimization. A practical method integrating FE modelling, Design of Experiments, and Response Surface optimization was developed to obtain optimal designs for cold roll formed steel sections in flexural strength considering distortional buckling failure. In particular, the FE model was developed for replicating the section's flexural behavior under four-point beam bending tests. The model included initial imperfections, geometry and the cold working effects for different stiffener shapes and was then utilized to optimize the buckling and flexural strength of the sections. Optimal cross-sectional shape of the longitudinally stiffened channel and zed sections was finally achieved. The following conclusions were drawn based on the results of this study:

1) The cold working had modest effect in material strength in the flat regions of cold roll formed steel sections by on average 2.5%, but significantly enhanced material strength in the corner and stiffener bend regions by on average 22%.

2) The results revealed the efficiency of the adopted optimization approach to increase the bending strength of cold roll formed sections. The ultimate moment capacities of the optimized sections were significantly higher than those obtained from their standard and reference counterparts for the same amount of material used. This improvement was more evident for the zed sections which were less prone to distortional-global buckling failure mode.

3) The cold working effect in the corner and stiffener areas was insignificant on bending strength in the standard sections and only had a relevant influence at reference sections bending strength. The main reason for the low contribution of the cold working effects can be the higher distortional buckling slenderness and the relatively small area of the rounded corners compared to the total cross section area in the sections. On the other hand, the cold working effect significantly increased the stiffness and bending strength of the optimized sections up to 7% and 6% for the channel and zed sections, respectively. In the optimized sections, several parts of the cross-section presented an equivalent strain higher than the yield strain, so the increase of the yield strength in corner areas produced an increase of the flexural strength of the beams.

4) When both geometry and the cold working effect were considered in the optimization process, optimal sections could be achieved with significant improvement in distortional buckling and ultimate strength. They were up to 84% and 20%, respectively, for the optimized channel section in comparison to the standard channel, and up to 105% and 23%, respectively, for the optimized zed section when compared to the standard zed section using the same amount of material.

5) The optimal cross-sectional shape recommended to have two longitudinal stiffeners at the web placed as much close as possible to the web-flange junctions, one longitudinal flange stiffeners placed near the web flange junctions as much as possible, and the relative dimensions of the sections as proposed in this paper. The proposed shape could gain significant benefit from the geometry and the cold working effects.

REFERENCES

[1] Ashraf M., Gardner L. and Nethercot D.A., "Strength enhancement of the corner regions of stainless steel cross-sections", *Journal of Constructional Steel Research*, **61**, 37-52, 2005.

[2] Gardner L. and Nethercot D.A., "Experiments on stainless steel hollow sections—Part 1: Material and cross-sectional behaviour", *Journal of Constructional Steel Research*, **60**, 1291-1318, 2004.

[3] Nguyen V.B., Pham C.H., Cartwright B. and English M., "Design of new cold rolled purlins by experimental testing and Direct Strength Method", *Thin-Walled Structures*, **118**, 105-112, 2017.

[4] B. Rossi, S. Afshan, L. Gardner, Strength enhancements in cold-formed structural sections—Part II: Predictive models, Journal of Constructional Steel Research 83 (2013) 189-196.

[5] Van der Merwe P. and van den Berg G., "Prediction of corner mechanical properties for stainless steels due to cold forming", *Eleventh International Specialty Conference on Cold-Formed Steel Structures*, St. Louis, Missouri, U.S.A., October 20-21, 1992.

[6] Karren K.W., "Corner properties of cold-formed shapes", *Journal of the Structural Division*, 93, 401-433, 1967.

[7] Haidarali M.R. and Nethercot D.A., "Local and distortional buckling of cold-formed steel beams with both edge and intermediate stiffeners in their compression flanges", *Thin-Walled Structures*, **54**, 106-112, 2012.

[8] Jandera M., Gardner L. and Machacek J., "Residual stresses in cold-rolled stainless steel hollow sections", *Journal of Constructional Steel Research*, **64**, 1255-1263, 2008.

[9] Nguyen V.B., Wang C., Mynors D., English M. and Castellucci M., "Compression tests of cold-formed plain and dimpled steel columns", *Journal of Constructional Steel Research*, **69**, 20-29, 2012.

[10] Nguyen V.B., Wang C., Mynors D., Castellucci M. and English M., "Finite element simulation on mechanical and structural properties of cold-formed dimpled steel", Thin-Walled Structures, **64**, 13-22, 2013.

[11] Nguyen V.B., Wang C., Mynors D., Castellucci M. and English M., "Analysis and design of cold-formed dimpled steel columns using Finite Element techniques", *Finite Elements in Analysis and Design*, **108**, 22-31, 2016.

[12] Wang F., "Numerical studies of residual stress in cold formed steel sigma sections", *PhD Thesis*, University of Birmingham, 2015.

[13] AISI, "North American specification for the design of cold-formed steel structural members", *AISI S100-16*, Washington DC, 2016.

[14] BSI, "Structural use of steelwork in building, Part 5: Code of practice for design of cold formed thin gauge sections", *British Standard Institution*, 1998.

[15] CEN, "1-3 Eurocode 3: Design of steel structures-Part 1-3: General rules - Supplementary rules for cold-formed members and sheeting", *European Committee for Standardization*, 2006.

[16] Nguyen V.B. and English M., "The optimization of thin-walled cold rolled products using Finite Element modelling and Design of Experiments", *The 8th International Conference on Thin-Walled Structures (ICTWS 2018)*, Lisbon, Portugal, 2018.

[17] Qadir S., Nguyen V.B., Hajirasouliha I., Cartwright B. and English M., "Optimal design of cold roll formed steel channel sections under bending considering both geometry and cold work effects", *Thin-Walled Structures*, **157**, 107020, 2020.

[18] Qadir S., Nguyen V.B., Hajirasouliha I., Cartwright B. and English M., "Optimisation of flexural strength for cold roll formed sections using design of experiments and response surface methodology", *Proceedings of the Cold-Formed Steel Research Consortium Colloquium*, 20-22 October, 2020.

[19] Qadir S., Nguyen V.B., Hajirasouliha I., Ceranic B., Tracada E. and English M., "Shape optimisation of cold roll formed sections considering effects of cold working", *Thin-Walled Structures*, **170**, 108576, 2022.